Pacific Northwest
NATIONAL LABORATORY

PNNL-39788

Preliminary Evaluation of the MAM4xx Aerosol Model Within the EAMxx Atmosphere (ne256; 12 km Resolution)

July 2026

Lead authors: Susannah Burrows[1], Balwinder Singh[1], Oscar Díaz-Ibarra[2], Meng Huang[1], Jeffrey Johnson[3], Jaelyn Litzinger[1], Naser Mahfouz[1], Taufiq Hassan[1], Johannes Mülmenstädt[1], James Overfelt[2], Michael J Schmidt[2], Kai Zhang[1]
1 – Pacific Northwest National Laboratory
2 – Sandia National Laboratory
3 – Cohere Consulting LLC

U.S. DEPARTMENT of ENERGY

Prepared for the U.S. Department of Energy
under Contract DE-AC05-76RL01830

DISCLAIMER

This report was prepared as an account of work sponsored by an agency of the United States Government. Neither the United States Government nor any agency thereof, nor Battelle Memorial Institute, nor any of their employees, makes **any warranty, express or implied, or assumes any legal liability or responsibility for the accuracy, completeness, or usefulness of any information, apparatus, product, or process disclosed, or represents that its use would not infringe privately owned rights**. Reference herein to any specific commercial product, process, or service by trade name, trademark, manufacturer, or otherwise does not necessarily constitute or imply its endorsement, recommendation, or favoring by the United States Government or any agency thereof, or Battelle Memorial Institute. The views and opinions of authors expressed herein do not necessarily state or reflect those of the United States Government or any agency thereof.

PACIFIC NORTHWEST NATIONAL LABORATORY
operated by
BATTELLE
for the
UNITED STATES DEPARTMENT OF ENERGY
under Contract DE-AC05-76RL01830

Printed in the United States of America

Available to DOE and DOE contractors from
the Office of Scientific and Technical Information,
P.O. Box 62, Oak Ridge, TN 37831-0062
www.osti.gov
ph: (865) 576-8401
fox: (865) 576-5728
email: reports@osti.gov

Available to the public from the National Technical Information Service
5301 Shawnee Rd., Alexandria, VA 22312
ph: (800) 553-NTIS (6847)
or (703) 605-6000
email: info@ntis.gov
Online ordering: http://www.ntis.gov

PNNL-39788

Preliminary Evaluation of the MAM4xx Aerosol Model Within the EAMxx Atmosphere (ne256; 12 km Resolution)

July 2026

Lead authors: Susannah Burrows[1], Balwinder Singh[1], Oscar Díaz-Ibarra[2], Meng Huang[1], Jeffrey Johnson[3], Jaelyn Litzinger[1], Naser Mahfouz[1], Taufiq Hassan Mozumder[1], Johannes Mülmenstädt[1], James Overfeldt[2], Michael J Schmidt[2], Kai Zhang[1]
1 – Pacific Northwest National Laboratory
2 – Sandia National Laboratory
3 – Cohere Consulting LLC

Prepared for
the U.S. Department of Energy
under Contract DE-AC05-76RL01830

Pacific Northwest National Laboratory
Richland, Washington 99354

Acknowledgments

We gratefully acknowledge the many individuals and organizations whose contributions made this work possible.

We thank the members of the Enabling Aerosol–Cloud Interactions at Global Convection-Permitting Scales (EAGLES) project for their essential work that produced the initial version of the MAM4xx code. Several members of that team are not coauthors of the current report, so we wish to explicitly acknowledge them by name: Po-Lun Ma, Jerome Fast, Kyle Pressel, Shuaiqi Tang, Brian Gaudet, Mingxuan Wu, Peter Bosler, and Andrew Salinger. The following authors of the current report also contributed to both the preceding EAGLES code porting effort and the current evaluation effort: Balwinder Singh, Oscar Díaz-Ibarra, Meng Huang, Jeffrey Johnson, Jaelyn Litzinger, Taufiq Hassan Mozumder, James Overfeldt, Michael Schmidt, and Kai Zhang.

We are grateful to the EAMxx team members who generously reviewed pull requests and provided technical feedback—in particular, Luca Bertagna and Conrad Clevenger. We also thank the broader Energy Exascale Earth System Model (E3SM) team, as well as the E3SM project's Executive Committee, including Peter Caldwell, Ruby Leung, and Mark Taylor, for their feedback, guidance and support.

We also extend our appreciation to the many colleagues who have contributed to the broader E3SM project but are not listed as authors of this report. The success of each individual effort within the E3SM project rests on the collective efforts of a much broader team, and we are grateful for the contributions of the large number of colleagues who have been instrumental to the E3SM project's success.

This research used resources of the National Energy Research Scientific Computing Center, a U.S. Department of Energy Office of Science user facility, through computing allocations on the Perlmutter system. We also used resources of the Oak Ridge Leadership Computing Facility, specifically the Frontier system, supported by the Office of Science of the U.S. Department of Energy.

Acronyms and Abbreviations

ACI	aerosol–cloud interactions
AOD	aerosol optical depth
BC	black carbon
CCN	cloud condensation nuclei
CEDS	Community Emissions Data System
CIME	Common Infrastructure for Modelling the Earth
CMIP	Coupled Model Intercomparison Project
CRUNCEP	Climate Research Unit - National Centers for Environmental Prediction
DOE	Department of Energy
E3SM	Energy Exascale Earth System Model
IMPACT	Integrated Massively Parallel Atmospheric Chemical Transport
MAM	Modal Aerosol Module
MIRAGE	Model for Integrated Research on Atmospheric Global Exchange
NERSC	National Energy Research Scientific Computing Center
POM	primary organic matter
S2D	seasonal-to-decadal
S2S	subseasonal-to-seasonal
SDPD	simulated days per wall-clock day
SPA	Simple Prescribed Aerosol
SYPD	simulated years per day
ZM	Zhang-McFarlane

Contents

Acknowledgments ii
Acronyms and Abbreviations iii
1.0 Introduction 1
2.0 Simulation Description 2
3.0 Aerosol Life Cycle 3
4.0 Aerosol Radiative Effects with MAM4xx and SPA 7
5.0 Computational Performance 9
5.1 Overall Computational Performance of EAMxx-MAM4xx 9
5.2 Performance of MAM4-EAMv2 vs. EAMxx-MAM4xx 10
5.3 Performance of MAM4xx CPU vs. GPU 11
5.4 Strong-Scaling Results for EAMxx-MAM4xx at ne256pg2 Resolution 12
6.0 Unit and System-Level Testing 14
7.0 Summary and Outlook 15
8.0 References 16

Figures

Figure 3.1 Simulated column burdens of different aerosol species (units: kg m^{-2}) from the ne256pg2L128 simulation. 5
Figure 3.2 Evaluation of simulated annual mean AOD at 550 nm from the MAM4xx ne256pg2 experiment (center), compared against the MACv2 aerosol climatology composite (Kinne et al., 2019) (top). 5
Figure 3.3 In the absence of the ZM convection parameterization, aerosol burdens are substantially higher across all species. The figure shows relative differences in aerosol burden between the reference EAMv3.HR simulation at ne256 (control, CTRL) and the sensitivity simulation without the ZM convective parameterization (noZM). Red color indicates increased aerosol burden in noZM. 6
Figure 4.1 The aerosol effective radiative forcing (ERF_{aer}) components are plotted temporally for both the MAM and SPA setups. 8
Figure 4.2 The aerosol effective radiative forcing (ERF_{aer}) components, plotted spatially for both the MAM and SPA setups. 8
Figure 5.1 Variation in the SYPD for the EAMxx-MAM4xx and default EAMxx ne30pg2 cases, reported daily at NERSC Performance Portal. 9
Figure 5.2 Variation in the SYPD for the EAMxx-MAM4xx and default EAMxx ne30pg2 cases, reported daily at Compy's Portal. 10
Figure 5.3 Wall-clock time per compute task of MAM4 processes, comparing EAMxx-MAM4xx and EAM-MAM4 (E3SM version 2, branch maint-2.0) at ne30 resolution, using 512 threads on Perlmutter CPUs (4 nodes). Blue bars represent MAMf90 with the default E3SM version 2 configuration

and sub-cycling of 6; orange bars represent MAMf90 with sub-cycling of 12; and green bars represent MAM4xx with sub-cycling of 12. Note that only the ACI process is part of the sub-cycling loop. 11

Figure 5.4 Strong-scaling performance (simulated days per wall-clock day [SDPD]) versus number of nodes for the EAMxx-MAM4xx configuration at ne30 resolution on Perlmutter, comparing GPU (solid lines, NPROC = 4–42) and CPU (dotted lines, NPROC = 128–1024) runs. Component SDPD is color-coded: atmosphere (green), which includes the dynamical core (red) and physics (purple), with the MAM4xx aerosol module (blue) embedded within physics. Scaling methodology follows Donahue et al. (2024). 12

Figure 5.5 Strong-scaling performance (SDPD) versus number of nodes for the EAMxx-MAM4xx configuration at ne256 resolution on Perlmutter. Component SDPD is color-coded: atmosphere (green), which includes the dynamical core and physics, with the MAM4xx aerosol module (red) embedded within physics. Scaling methodology follows Donahue et al. (2024). Each node has four A100 NVIDIA GPUs. 13

Tables

Table 3.1 Burden, lifetime, and mass budgets of various types of aerosols simulated by MAM4xx at ne256L128 resolution. Note that the total source includes the contribution from chemical production. Values in brackets are AeroCom Phase III multi-model median results. For the POM burden, the AeroCom median value is the total organic aerosol burden. 4

1.0 Introduction

The Department of Energy (DOE) is preparing its Energy Exascale Earth System Model (E3SM) for its fourth major release (E3SMv4, targeted for 2028), with the overarching goal of advancing predictive capabilities for energy-relevant Earth system processes across subseasonal-to-seasonal (S2S) and seasonal-to-decadal (S2D) timescales. Aerosol–cloud–radiation interactions represent an important source of uncertainty and model bias in S2S and S2D predictions with physical models, influencing regional precipitation phase, intensity, and amount, as well as regional energy budgets, on the timescales most relevant to DOE's mission. Faithfully representing these interactions within the E3SM requires an interactive aerosol module that captures the dynamic feedback between aerosol sources, atmospheric transformations, removal processes, and aerosol–cloud interactions (ACI).

To support these scientific objectives, the E3SM project will add an interactive aerosol module as part of an incremental update to E3SMv4 (i.e., E3SMv4.X). In preparation, a GPU-enabled version of the Modal Aerosol Module's four-mode configuration (MAM4), called MAM4xx, has recently been integrated into EAMxx, the newly developed C++ atmosphere component of E3SM. Currently EAMxx simulations performed in the model's default configuration use the Simple Prescribed Aerosol (SPA) scheme (Mahfouz et al., 2025), which provides computationally efficient, precomputed aerosol forcing fields but cannot capture the interactive feedback between aerosol processes and the atmospheric state. MAM4xx addresses this limitation by explicitly simulating the full aerosol life cycle—emissions, gas-phase and aqueous-phase chemistry, microphysical aging, intermodal transfer, transport, and dry and wet deposition—thereby enabling physically based aerosol couplings with clouds, radiation, land surfaces, and ocean biogeochemistry.

MAM4xx is a direct port of MAM4, from the Fortran-based E3SMv2 version into performance-portable C++ for use within EAMxx. The modal design traces its lineage through a series of predecessors: the Model for Integrated Research on Atmospheric Global Exchange (MIRAGE) model (Ghan et al., 2001; Easter et al., 2004), the Integrated Massively Parallel Atmospheric Chemical Transport (IMPACT) model (Herzog et al., 2004; Liu et al., 2005; Wang et al., 2009), and the MAM3/MAM7 implementations in the Community Earth System Model (Liu et al., 2012), leading to the MAM4 configuration described in Liu et al. (2016). E3SMv1 introduced additional aerosol features (Rasch et al., 2019; Wang et al., 2020), and the E3SMv2 MAM4, which forms the basis for MAM4xx, is largely identical to the E3SMv1 code (Zhang et al., 2022). Several additional aerosol developments were carried out separately for E3SMv3 (Golaz et al., 2025; Xie et al., 2025); these are not part of the current MAM4xx implementation. MAM4xx is planned for incorporation into the E3SMv4.x release, an incremental update following the initial v4.0 delivery, allowing for continued development and tuning before its inclusion in production configurations.

This report documents a preliminary evaluation of MAM4xx within EAMxx at approximately 12 km horizontal resolution (ne256pg2), representing the first comprehensive high-resolution assessment of MAM4xx aerosol budgets, radiative forcing, and ACI). The preliminary evaluation was requested by the E3SM project's executive committee to support project planning and the completion of the EAMv4 release. It built on earlier aerosol modeling work within E3SM at coarser resolutions. Through a combination of paired MAM4xx–SPA comparisons, multi-resolution experiments, and targeted sensitivity studies, this evaluation identified the principal biases in the current MAM4xx implementation, diagnosed their likely causes, and outlined priorities for the next phase of development.

2.0 Simulation Description

The primary simulations evaluated in this report were conducted with a development version of EAMxx-MAM4xx (commit hash: fa2d97d) configured at ne256pg2 horizontal resolution (approximately 12 km) with 128 vertical levels (ne256pg2L128). The simulations covered a 13-month integration initialized on August 1, 2019, with the first month discarded as spin-up, yielding a September 2019 through August 2020 analysis period. Sea surface temperature was prescribed from the Operational Sea Surface Temperature and Ice Analysis, and the sea ice coverage was obtained from The European Organization for the Exploitation of Meteorological Satellite Ocean and Sea Ice Satellite Application Facility. Atmospheric initial conditions were derived from ERA5 reanalysis at 0.25°×0.25° and interpolated to the EAMxx grid and vertical levels. Initial land conditions were generated from an off-line land model spin-up forced by the Climate Research Unit – National Centers for Environmental Prediction (CRUNCEP) dataset (Viovy, 2018) following Mahfouz et al. (2025). Aerosols were initialized from a preceding 1-year simulation. Emissions of aerosols and their precursors were obtained from Coupled Model Intercomparison Project (CMIP) phase 6 (CMIP6) emission datasets, including anthropogenic emissions from the Community Emissions Data System ([CEDS] Hoesly et al., 2018) and biomass burning emissions for CMIP6 ([BB4CMIP] van Marle et al., 2017). Boundary conditions were based on the standard EAMv2 F2010 configuration for present-day scenarios. To constrain large-scale circulation, zonal and meridional winds were nudged toward MERRA-2 reanalysis with a 6-hour relaxation timescale. Tropospheric oxidants were prescribed based on the CMIP6 ozone database (Hegglin et al., 2018). A companion MAM4xx simulation using pre-industrial emissions was also conducted to facilitate present-day versus pre-industrial (PD–PI) diagnostics for aerosol radiative forcing calculations.

Parallel simulations using the SPA scheme at the same resolution and nudging configuration were conducted to provide a direct baseline comparison, enabling isolation of the impacts of transitioning from prescribed to interactive aerosols on aerosol optical depth (AOD), cloud droplet number concentration, cloud radiative effects, and precipitation. In addition, supplementary experiments explored two dimensions of sensitivity. First, simulations at multiple horizontal and vertical resolutions (ne256pg2L128, ne30pg2L72, and ne30pg2L128) were conducted within EAMxx-MAM4xx and compared against E3SMv2 at ne30L72 to evaluate the resolution dependence of aerosol budgets and removal processes. Second, experiments within EAMv3 at high resolution (ne256), with and without the Zhang-McFarlane (ZM) convective parameterization, were analyzed to isolate the role of convective transport and wet removal.

3.0 Aerosol Life Cycle

The aerosol life cycle in MAM4xx encompasses the chain of processes governing atmospheric aerosol populations:

- emission from natural and anthropogenic sources (including precursor gases)
- gas-to-particle conversion
- chemical transformation (including aqueous-phase processing in cloud droplets)
- microphysical aging and intermodal transfer
- transport by resolved and parameterized motions
- removal by dry deposition and wet scavenging.

Three primary diagnostics were used to assess the fidelity of this life cycle. The column-integrated aerosol burden (mass per unit area for each species) reflects the combined effects of emissions, chemical production, transport, and removal. Aerosol lifetime, defined as the ratio of global burden to total removal rate, indicates the mean residence time in the atmosphere. The global mass budget quantifies the balance of sources and sinks for each species. These are standard metrics for global aerosol model intercomparisons, and they were evaluated against (present-day) multi-model ranges from the Phase III AeroCom intercomparison project (Gliß et al., 2021).

Global budgets and burden biases. Table 3.1 summarizes the global annual mean aerosol burdens, lifetimes, and mass budget terms for the major aerosol species simulated by MAM4xx at ne256L128 resolution, and Figure 3.1 provides maps of the simulated column burdens (in kg m^{-2}) for individual species. MAM4xx reproduces the expected spatial patterns—elevated burdens over industrial regions, biomass burning zones, and deserts—but the magnitudes of column burdens and lifetimes for key anthropogenic and biogenic species are systematically high relative to AeroCom benchmarks. For black carbon (BC), the simulated global burden of 0.46 Tg substantially exceeds the AeroCom Phase III range of approximately 0.1–0.3 Tg, and the lifetime of 15 days lies well above the AeroCom III range of approximately 3–10 days. Similar positive biases in burden and lifetime were found for primary organic matter (POM), sulfate, and secondary organic aerosol.

AOD evaluation. The elevated burdens translate directly into high biases in aerosol optical depth, as shown in Figure 3.2, which compares simulated annual mean AOD at 550 nm from the MAM4xx ne256pg2 experiment against the MACv2 aerosol climatology composite (Kinne et al., 2019). The AOD bias is most pronounced in the Northern Hemisphere, downwind of major anthropogenic and biomass burning source regions, where simulated AOD substantially exceeds the MACv2 reference. Over remote ocean regions and the Southern Hemisphere, where natural species (sea salt and dust) dominate, the biases are comparatively smaller. This geographic pattern—with the strongest biases occurring where fine-mode anthropogenic aerosol dominates—is consistent with the hypothesis that the primary issue lies in insufficient removal rather than in emission or optical property errors.

Wet removal deficiency and the role of convection. Multiple lines of evidence point to inefficient wet removal as the primary root cause of the excess burdens and lifetimes. It was hypothesized that these biases would be reduced by the addition of the ZM convection parameterization to EAMxx, an effort that is currently underway and planned for completion in

2026. To test this hypothesis, sensitivity experiments were conducted within EAMv3 at high resolution (EAMv3.HR, ne256), with and without the ZM convective parameterization. These simulations demonstrated that in the absence of ZM, aerosol burdens were substantially higher across all species (Figure 3.3). The relative increase in burden upon removing ZM ranged from approximately 21 percent for dust to 72 percent for POM, with sulfate burden increasing by roughly 45 percent and BC by approximately 69 percent. These results confirm that adding ZM to EAMxx is likely to improve the simulated aerosol life cycle.

Additionally, multi-resolution analysis demonstrated that the wet removal deficiency is intrinsic to the EAMxx-MAM4xx implementation rather than solely a consequence of high resolution: burden biases were even larger at ne30 than at ne256, indicating that differences in process coupling, time-stepping, or parameterization details in MAM4xx relative to E3SMv2 also contribute to the high AOD bias.

Addressing the wet removal bias through a combination of ZM coupling, parametric calibration, and possible reformulation of wet scavenging treatments is a significant focus of current efforts.

Table 3.1 Burden, lifetime, and mass budgets of various types of aerosols simulated by MAM4xx at ne256L128 resolution. Note that the total source includes the contribution from chemical production. Values in brackets are AeroCom Phase III multi-model median results. For the POM burden, the AeroCom median value is the total organic aerosol burden.

Species	Burden (Tg)	Total Sources & Sinks (Tg yr^{-1})	Emissions (Tg yr^{-1})	Dry dep. (Tg yr^{-1})	Wet dep. (Tg yr^{-1})	Lifetime (days)
BC	0.46 (0.13)	+9.48 / −11.0	9.48 (9.7)	−2.90	−8.10	15.2 (5.5)
POM	2.60 (1.9*)	+47.7 / −57.9	47.7 (N/A)	−14.8	−43.1	16.4 (6.0*)
SO_4 (TgS)	2.37 (0.6)	+59.8 (47.6) / −69.9	1.80 (N/A)	−11.0	−58.8	12.4 (4.9)
SOA	6.64 (N/A)	+88.7 / −108	—	−16.0	−91.6	22.5 (N/A)
Sea salt	9.55 (8.7)	+2305 / −2445	2305 (4980)	−1271	−1174	1.43 (0.56)
Dust	25.8 (16.6)	+1550 / −1657	1550 (1440)	−1285	−372	5.69 (3.7)

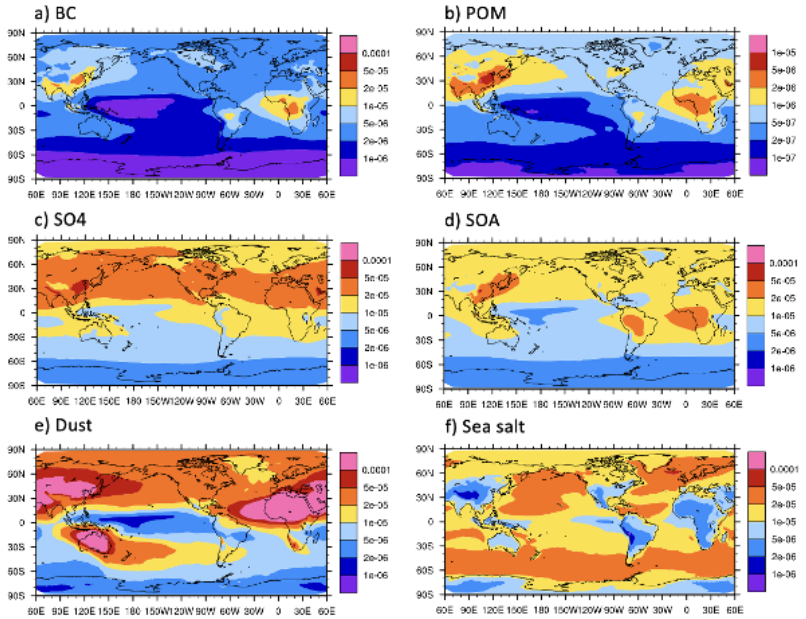

Figure 3.1 Simulated column burdens of different aerosol species (units: kg m^{-2}) from the ne256pg2L128 simulation.

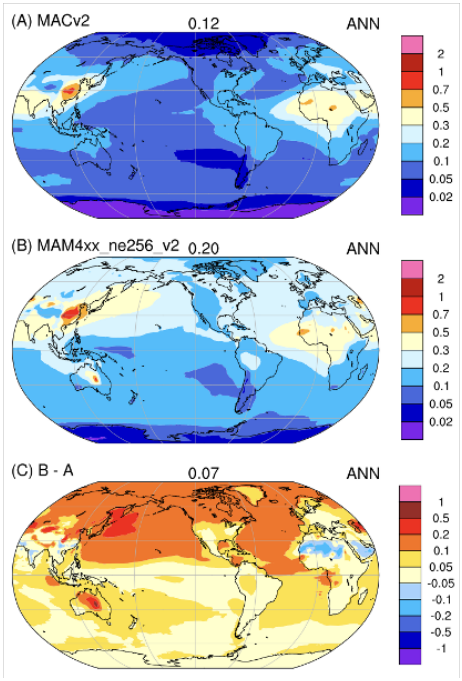

Figure 3.2 Evaluation of simulated annual mean AOD at 550 nm from the MAM4xx ne256pg2 experiment (center), compared against the MACv2 aerosol climatology composite (Kinne et al., 2019) (top).

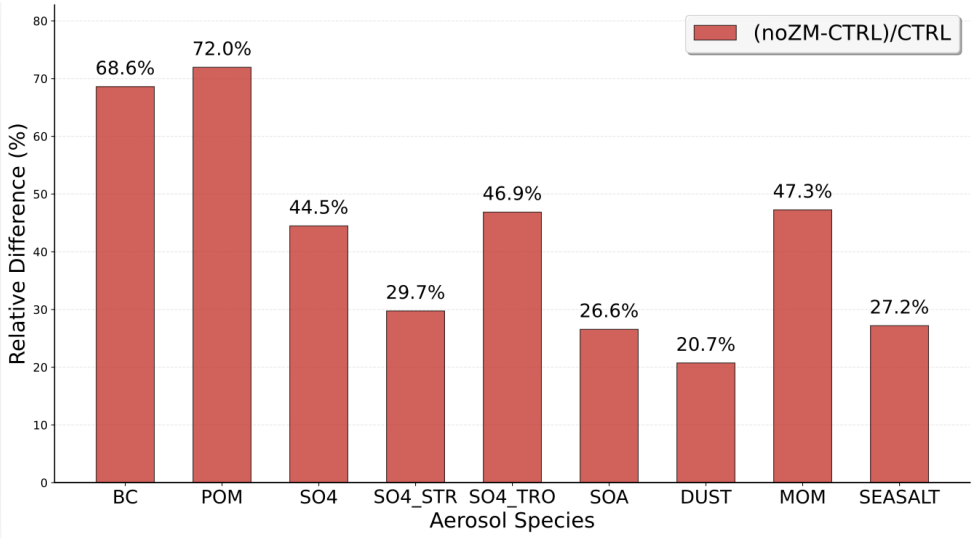

Figure 3.3 In the absence of the ZM convection parameterization, aerosol burdens are substantially higher across all species. The figure shows relative differences in aerosol burden between the reference EAMv3.HR simulation at ne256 (control, CTRL) and the sensitivity simulation without the ZM convective parameterization (noZM). Red color indicates increased aerosol burden in noZM.

4.0 Aerosol Radiative Effects with MAM4xx and SPA

The effective radiative forcing of aerosols (ERF_{aer}) quantifies the net radiative impact of aerosol perturbations and is a key metric for evaluating the prediction-relevant performance of MAM4xx. ERF_{aer} is decomposed into contributions from aerosol–radiation interactions (ERF_{ari}), capturing direct scattering and absorption by aerosol particles, and ACI (ERF_{aci}), encompassing the microphysical effects of aerosols on cloud droplet number, cloud albedo, liquid water path, and precipitation. Both components were quantified using paired present-day and pre-industrial simulations for the MAM4xx and SPA configurations.

Magnitude and temporal evolution. Figure 4.1 presents the seasonal cycle of ERF_{aer} and its decomposition into its components, ERF_{aci}, ERF_{ari}, and ERF_{res}. The annual mean ERF_{aci} in EAMxx-MAM4xx was -2.07 W m^{-2}, substantially more negative than the -1.23 W m^{-2} obtained with SPA—a difference of 0.84 W m^{-2}, indicating much stronger cloud-mediated cooling with interactive aerosols. The ERF_{ari} was +0.26 W m^{-2} for MAM4xx, compared to +0.06 W m^{-2} for SPA, consistent with the higher aerosol loading described in Section 3.0. Residual terms (ERF_{res}) were small in both cases (+0.04 W m^{-2} for MAM4xx, +0.08 W m^{-2} for SPA). The overall ERF_{aer} was thus dominated by the ERF_{aci} component, with ACI exerting a forcing roughly an order of magnitude larger than the direct aerosol–radiation effect.

Spatial patterns. The geographic distribution of ERF_{aer} components (Figure 4.2) reflects the spatial patterns of aerosol loading, with the strongest forcing signals collocated with major anthropogenic source regions and their downwind marine environments. MAM4xx produced a much stronger ERF_{aci} signal in regions with persistent marine stratocumulus decks—e.g., off the coasts of California and Chile. Current efforts focus on detailed evaluation and improvement of the physical ACI mechanisms in preparation for the E3SMv4.X release.

Longwave ERF_{aci} anomaly. An unexpected feature is a negative global mean longwave ERF_{aci}, with a sign opposite to that typically produced by ACI (-0.90 W m^2). In past versions of E3SM, aerosol effects on warm clouds produced a modest positive or near-zero longwave forcing. The negative longwave ERF_{aci} in MAM4xx may be related to the representation of heterogeneous ice nucleation, which can modify upper-tropospheric ice cloud properties and their longwave emission, particularly in the tropics. The mechanisms underlying this behavior remain an open question requiring further investigation.

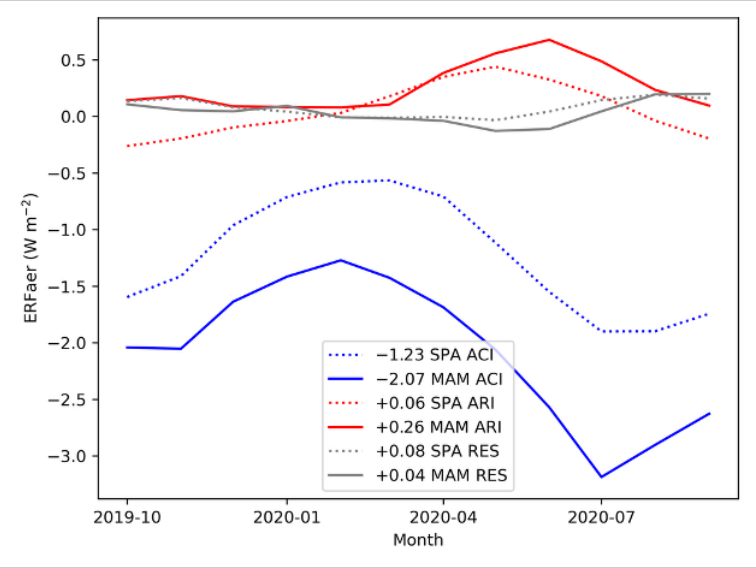

Figure 4.1 The aerosol effective radiative forcing (ERF_{aer}) components are plotted temporally for both the MAM and SPA setups.

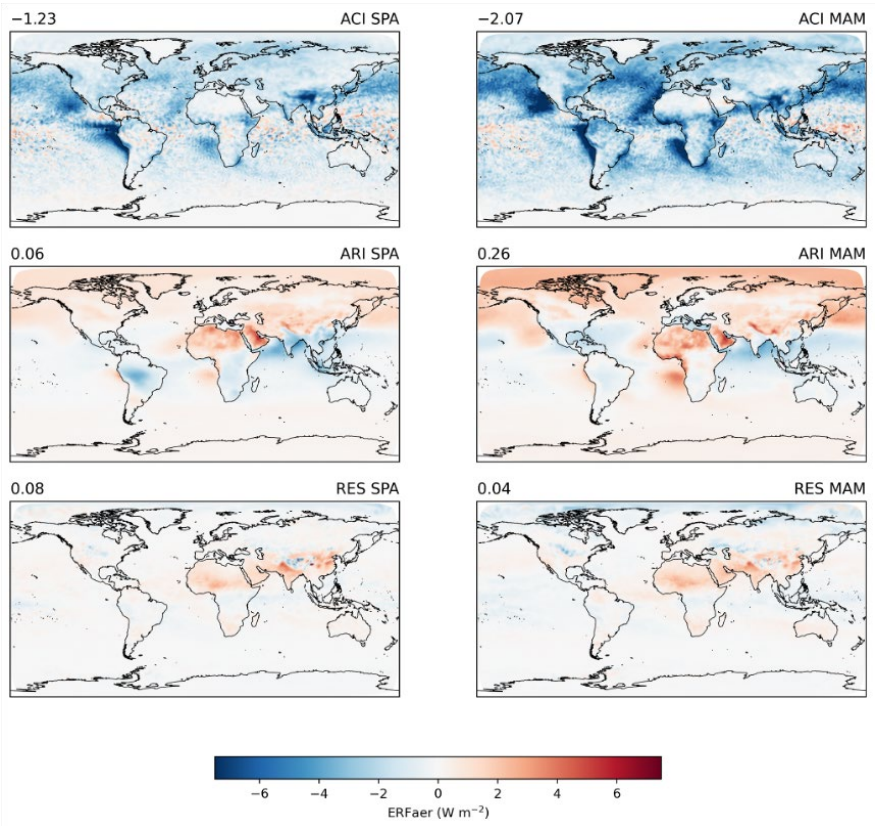

Figure 4.2 The aerosol effective radiative forcing (ERF_{aer}) components, plotted spatially for both the MAM and SPA setups.

5.0 Computational Performance

This section details our evaluation of the computational overhead and scaling behavior introduced by the fully interactive MAM4xx aerosol model in EAMxx. We first quantified the runtime increase when replacing the default SPA-based aerosol treatment with MAM4xx on two platforms: Perlmutter (GPU) and Compy (CPU). Next, we performed a head-to-head comparison of the new Kokkos/C++ MAM4xx code against the Fortran MAMf90 implementation at ne30pg2 resolution. We then analyzed GPU-specific performance trade-offs, showing how the modest slowdown of the aerosol component is outweighed by dramatic GPU speedups in the dynamical core. Finally, we conducted a strong-scaling study at ne256pg2 resolution to assess parallel efficiency up to 1,000 nodes.

5.1 Overall Computational Performance of EAMxx-MAM4xx

Integrating a more comprehensive aerosol treatment via MAM4xx introduced a notable computational cost to EAMxx. We measured overall performance, defined as simulated years per day (SYPD), for the EAMxx-MAM4xx configuration nightly on two platforms: Compy, a CPU-based machine at Pacific Northwest National Laboratory, and Perlmutter, an NVIDIA GPU-based machine at the National Energy Research Scientific Computing Center (NERSC). As a baseline, we also reported SYPD for the default EAMxx configuration. Each test was run at ne30pg2 and ne4pg2 resolutions for a simulation length of 5 days. Figures 5.1 and 5.2 display dashboards for Perlmutter and Compy, respectively, where each data point shows the SYPD achieved by a single simulation (y-axis) on a specific date (x-axis). On Perlmutter, the EAMxx-MAM4xx configuration achieved 5 SYPD compared to 18 SYPD for the default configuration, reflecting a 3.6× increase in computational cost. Similarly, on Compy, EAMxx-MAM4xx achieved 0.3 SYPD versus 0.5 SYPD for the default configuration, a 1.6× increase in cost.

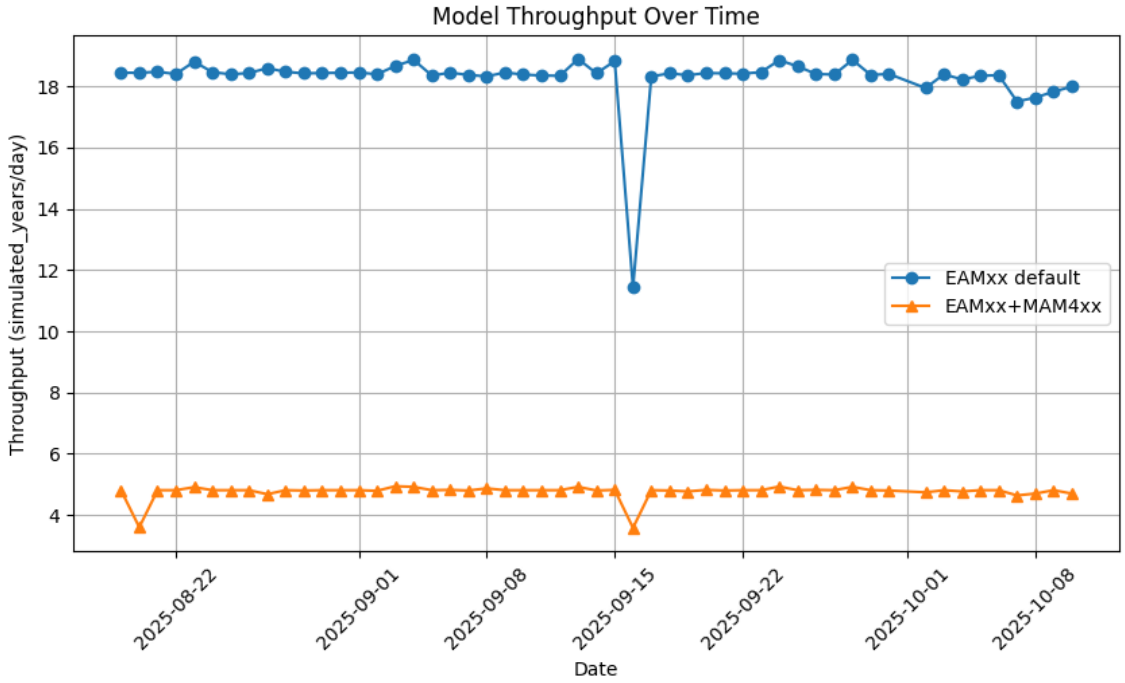

Figure 5.1 Variation in the SYPD for the EAMxx-MAM4xx and default EAMxx ne30pg2 cases, reported daily at NERSC Performance Portal.

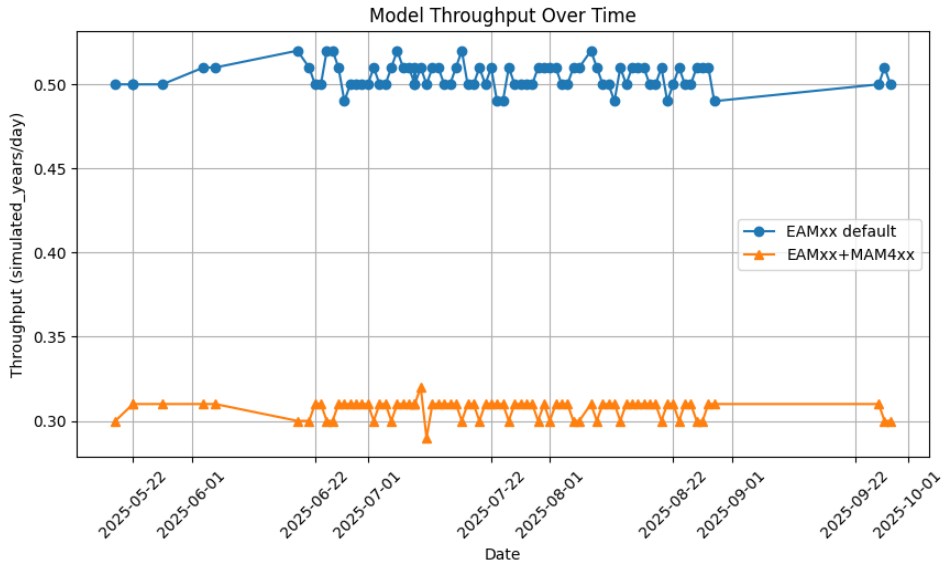

Figure 5.2 Variation in the SYPD for the EAMxx-MAM4xx and default EAMxx ne30pg2 cases, reported daily at Compy's Portal.

The computational disparity between the default EAMxx configuration and EAMxx-MAM4xx stems from fundamental architectural differences. The default setup uses the SPA scheme to read precomputed fields for radiation and cloud condensation nuclei (CCN) concentrations, greatly simplifying the simulation. In contrast, EAMxx-MAM4xx explicitly represents seven aerosol-relevant processes, yielding a more realistic depiction of aerosol dynamics at the expense of higher computational cost.

5.2 Performance of MAM4-EAMv2 vs. EAMxx-MAM4xx

After completing the port of MAMf90 Fortran code to Kokkos/C++, we evaluated the performance of MAM4xx relative to the original implementation. To this end, simulations were conducted at ne30pg2 resolution using E3SM version 2 for the Fortran-based case and the EAMxx-MAM4xx compset on the Perlmutter supercomputer at NERSC.

We found that the performance of MAM4xx is similar to that of MAMf90 on CPUs when the same sub-cycling values are used for both configurations. There are several differences between the E3SM version 2 and the EAMxx-MAM4xx configurations; however, we focused only on those relevant to MAM4. Specifically, in the MAMf90 configuration, the ACI process is part of an inner loop referred to as sub-cycling, and different default sub-cycling values are used by E3SM version 2 and EAMxx-MAM4xx. To ensure a fair comparison between the Fortran and C++ implementations, we used the same sub-cycling value and compared only the MAM4 processes, which include ACI, wet scavenging, aerosol optics, surface online emissions, aerosol microphysics, and dry deposition. As shown in Figure 5.3, the total wall-clock time was similar across all MAM4 processes, except for ACI, where sub-cycling had a notable impact, as expected: a larger number of sub-cycling iterations results in an increased number of model evaluations for ACI. Finally, in terms of SYPD, the Fortran case was slightly faster than the C++ case, achieving 5.02 SYPD compared to 4.65 SYPD.

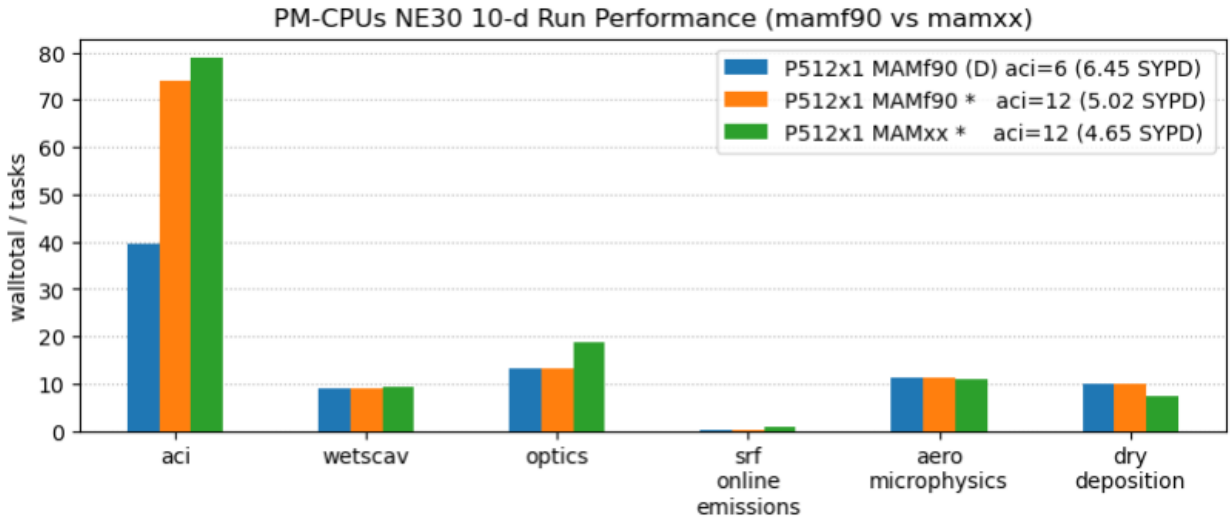

Figure 5.3 Wall-clock time per compute task of MAM4 processes, comparing EAMxx-MAM4xx and EAM-MAM4 (E3SM version 2, branch maint-2.0) at ne30 resolution, using 512 threads on Perlmutter CPUs (4 nodes). Blue bars represent MAMf90 with the default E3SM version 2 configuration and sub-cycling of 6; orange bars represent MAMf90 with sub-cycling of 12; and green bars represent MAM4xx with sub-cycling of 12. Note that only the ACI process is part of the sub-cycling loop.

5.3 Performance of MAM4xx CPU vs. GPU

We evaluated the computational performance of the EAMxx-MAM4xx configuration on both CPUs and GPUs. Figure 5.4 presents strong-scaling results for four components: MAM4xx aerosol (blue), physics (purple), dynamical core (red), and atmosphere (green), with solid lines for GPU runs and dotted lines for CPU runs. Contrary to expectations, the GPU implementation (blue solid lines) of MAM4xx was slightly slower than its CPU counterpart (blue dotted lines). Despite this modest GPU slowdown in the aerosol component, the overall configuration still achieved greater SYPD on GPUs because the dynamical core runs substantially faster. The current MAM4xx code is a direct Fortran port without any GPU-specific optimizations; future work will focus on accelerating the three most expensive processes (ACI, wet scavenging, and aerosol microphysics) on GPUs.

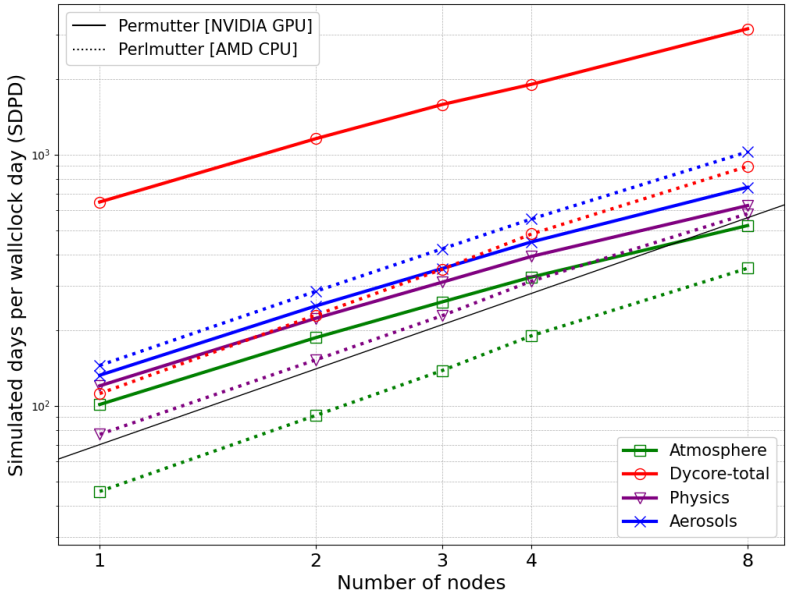

Figure 5.4 Strong-scaling performance (simulated days per wall-clock day [SDPD]) versus number of nodes for the EAMxx-MAM4xx configuration at ne30 resolution on Perlmutter, comparing GPU (solid lines, NPROC = 4–42) and CPU (dotted lines, NPROC = 128–1024) runs. Component SDPD is color-coded: atmosphere (green), which includes the dynamical core (red) and physics (purple), with the MAM4xx aerosol module (blue) embedded within physics. Scaling methodology follows Donahue et al. (2024).

5.4 Strong-Scaling Results for EAMxx-MAM4xx at ne256pg2 Resolution

To evaluate how well the EAMxx-MAM4xx configuration scales, we conducted a strong-scaling test at the target resolution of ne256pg2. In strong scaling, the total problem size remains fixed while the number of computational nodes is increased, allowing us to assess how efficiently the model reduces time-to-solution with more resources. As shown in Figure 5.5, the SDPD increased as the number of nodes scaled from 128 (512 GPUs) to 256 (1024 GPUs), demonstrating that the model effectively leverages additional compute resources. While the observed performance does not perfectly follow the ideal linear scaling curve, primarily because of communication overhead and other parallelization limits, the trend is close to linear, particularly between 512 and ~960 GPUs. At higher GPU counts, the gap between ideal and actual performance becomes more pronounced but remains moderate. Overall, this result is encouraging, as it confirms that EAMxx-MAM4xx maintains high parallel efficiency at scale, a critical requirement for high-resolution simulations on leadership-class GPU-based supercomputers.

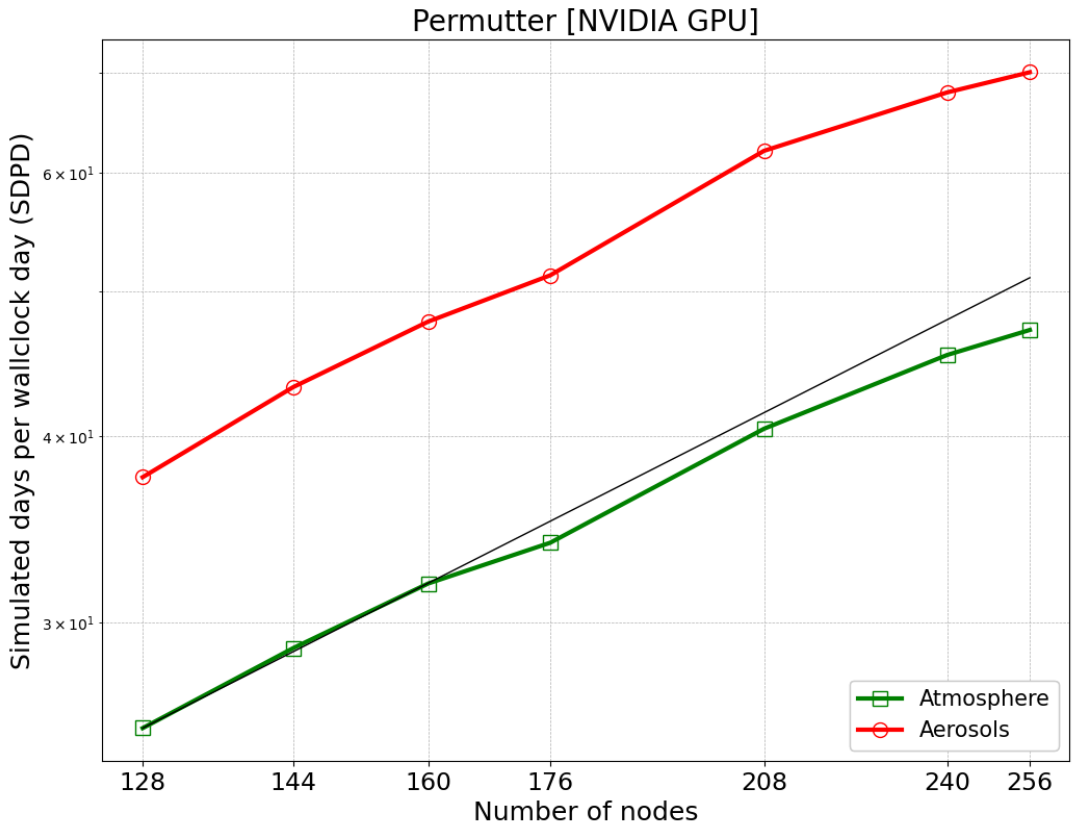

Figure 5.5 Strong-scaling performance (SDPD) versus number of nodes for the EAMxx-MAM4xx configuration at ne256 resolution on Perlmutter. Component SDPD is color-coded: atmosphere (green), which includes the dynamical core and physics, with the MAM4xx aerosol module (red) embedded within physics. Scaling methodology follows Donahue et al. (2024). Each node has four A100 NVIDIA GPUs.

6.0 Unit and System-Level Testing

Testing has been central to MAM4xx since inception and has included unit tests (individual functions/processes) and system-level tests (EAMxx-MAM4xx within the Common Infrastructure for Modelling the Earth [CIME]). MAM4xx uses GitHub Actions Continuous Integration to validate all new and existing code. Nearly 500 automated tests cover about 93 percent of the codebase, with nightly runs on the main branch to catch regressions and required tests before merging any new pull requests. Automated testing also ensures consistent behavior across compute architectures and build options. We test on CPUs, NVIDIA GPUs, AMD GPUs, and Intel GPUs across single and double precision modes, in both debug and release configurations. CPU tests are run on GitHub-hosted hardware; GPU tests are run on Sandia National Laboratories systems in containerized testing environments (Docker/Podman). Current GPU coverage includes NVIDIA H100 (CUDA) and AMD MI200/MI250 (HIP). At the system level, MAM4xx is tested nightly in the E3SM CIME framework using the F2010-EAMxx-MAM4xx compset across major E3SM platforms are used to verify stability over months-to-years timescales and include Bit-for-Bit restart and repeated testing in both debug and release modes. Finally, MAM4xx's modular "plug-and-play" processes (e.g., ACI, microphysics, wet scavenging, dry deposition) are explicitly exercised in nightly tests to ensure continued robustness and faster debugging.

7.0 Summary and Outlook

In this first comprehensive evaluation of the MAM4xx interactive aerosol module within EAMxx at approximately 12 km horizontal resolution (ne256pg2L128), we assessed the aerosol life cycle (Section 3.0), aerosol radiative effects and ACI (Section 4.0), and computational performance (Section 5.0) to establish a baseline understanding of MAM4xx capabilities and identify the principal challenges to be addressed before its incorporation into E3SMv4.x.

Key scientific findings. The aerosol life cycle evaluation revealed systematically high aerosol burdens and lifetimes for key anthropogenic and biogenic species—including BC, POM, sulfate, and secondary organic aerosol—relative to the AeroCom Phase III multi-model benchmarks. These biases translate into elevated AODs, particularly in the Northern Hemisphere. Multiple lines of evidence point to inefficient wet removal as the primary cause. The current EAMxx configuration at ne256 does not include the ZM convective parameterization, which provides a significant fraction of convective wet scavenging in earlier E3SM versions; disabling ZM in EAMv3 at comparable resolution increased aerosol burdens by 21–72 percent depending on species. Additionally, multi-resolution analysis demonstrated that the wet removal deficiency is not explained solely by moving to higher resolution: burden biases are even larger at ne30 than at ne256, indicating that other differences in EAMxx-MAM4xx relative to E3SMv2, beyond resolution differences alone, also contribute to the high AOD bias.

The aerosol radiative forcing evaluation found that ERF_{aci} dominates the overall ERF_{aer}, with a value of −2.07 W m^{-2} in MAM4xx compared to −1.23 W m^{-2} in SPA. An anomalously strong aerosol activation response—where a larger fraction of CCN is activated into cloud droplets than expected based on earlier versions of E3SM and other coarse-resolution (e.g., 1-degree) global models—was identified as a key contributor to the strong aerosol effective radiative forcing. A negative longwave ERF_{aci}, opposite in sign to typical model behavior, was also noted and may be connected to the representation of heterogeneous ice nucleation in MAM4xx.

Key technical findings. MAM4xx was successfully integrated and stabilized for yearlong simulations at ne256pg2 resolution, with over 60 pull requests merged to resolve stability issues. The C++ MAM4xx implementation achieves comparable or better wall-clock performance than the Fortran MAM4 for all processes except ACI, which is approximately 8 percent slower and remains the most expensive aerosol subcomponent. On Perlmutter GPUs, the EAMxx-MAM4xx configuration is approximately 3.6× more expensive than EAMxx-SPA, with wet scavenging identified as the primary GPU performance bottleneck. Strong-scaling results demonstrated that EAMxx-MAM4xx achieves near-linear parallel efficiency at the ne256pg2 target resolution, validating its readiness for high-resolution production runs on leadership-class GPU supercomputers.

Near-term priorities. Scientific priorities for the current phase of development center on two areas, informed by the findings in this preliminary evaluation. The first area of focus is improving the aerosol life cycle—particularly wet removal—through coupling MAM4xx to the ZM convective parameterization (when available in EAMxx), implementing parametric tunings analogous to those in EAMv3, and evaluating oxidant fields for consistency with model meteorology. The second focus is diagnosing and resolving the aerosol activation and ACI biases through N_c budget analysis, updraft velocity evaluation, and targeted comparisons across model versions. Technical priorities include identifying and addressing performance bottlenecks at ne256pg2 and ne1024pg2 resolutions, expanding GPU-specific profiling, refactoring computational hotspots, ensuring stable multiyear simulations with reliable restart functionality, and implementing additional physics features including the ZM coupling.

8.0 References

Donahue, A. S., P.M. Caldwell, L. Bertagna, H. Beydoun, P. A. Bogenschutz, A. M. Bradley, et al. 2024. “To exascale and beyond—The Simple Cloud-Resolving E3SM Atmosphere Model (SCREAM), a performance portable global atmosphere model for cloud-resolving scales.” *Journal of Advances in Modeling Earth Systems* 16: e2024MS004314. https://doi.org/10.1029/2024MS004314

Easter, R. C., S. J. Ghan, Y. Zhang, R. D. Saylor, E. G. Chapman, N. S. Laulainen, H. Abdul-Razzak, L. R. Leung, X. Bian, and R. A. Zaveri. 2004. “MIRAGE: Model description and evaluation of aerosols and trace gases., *J. Geophys. Res.* 109 D20210. https://doi.org/10.1029/2004JD004571

Fast, J. D., Singh, B., Diaz-Ibarra, O., Johnson, J., Dhandapani, C., Gaudet, B., Hassan, T., Huang, M., Litzinger, J., Overfelt, J., Pressel, K., Schmidt, M., Tang, S., Varble, A. C., Wan, H., Wu, M., Zhang, K., and Ma, P.-L.: The 4-mode Modal Aerosol Module in C++ (MAM4xx) v1.0: Representing Prognostic Aerosols in a Global Cloud-System Resolving Atmosphere Model for GPU Exascale Computing, EGUsphere [preprint], https://doi.org/10.5194/egusphere-2026-1538, 2026.

Gettelman, A., X. Liu, D. Barahona, U. Lohmann, and C. Chen. 2012. “Climate impacts of ice nucleation.” *J. Geophys. Res*. 117: D20201. https://doi.org/10.1029/2012JD017950.

Ghan, S. J., R.C. Easter, E. G. Chapman, H. Abdul-Razzak, Y. Zhang, L. R. Leung, N. S. Laulainen, R. D. Saylor, and R. A. Zaveri. 2001. “A physically based estimate of radiative forcing by anthropogenic sulfate aerosol.” *Journal of Geophysical Research: Atmospheres*, *106* (D6): 5279–5293.

Ghan, S. J. and R. C. Easter. 2006. “Impact of cloud-borne aerosol representation on aerosol direct and indirect effects.” *Atmos. Chem. Phys*. 6: 4163–4174. doi:10.5194/acp-6-4163-2006

Ghan, S. J. 2013. “Estimating aerosol effects on cloud radiative forcing.” *Atmospheric Chemistry and Physics* 13 (19): 9971–9974. https://doi.org/10.5194/acp-13-9971-2013

Gliß, J., A. Mortier, M. Schulz, M., et al. 2021. “AeroCom phase III multi-model evaluation of the aerosol life cycle and optical properties using ground- and space-based remote sensing as well as surface in situ observations.” *Atmos. Chem. Phys*. 21 87–128. https://doi.org/10.5194/acp-21-87-2021

Golaz, Jean-Christophe, Peter M. Caldwell, Luke P. Van Roekel, Mark R. Petersen, Qi Tang, Jonathan D. Wolfe, Guta Abeshu et al. "The DOE E3SM coupled model version 1: Overview and evaluation at standard resolution." *Journal of Advances in Modeling Earth Systems* 11, no. 7 (2019): 2089-2129.

Hegglin, M. I., D. Kinnison, D. Plummer, and K. P. Shine. 2018. “CMIP6 Ozone Forcing Dataset.” https://doi.org/10.5281/zenodo.1135127

Herzog, M., D. K. Weisenstein, and J. E. Penner. 2004. “A dynamic aerosol module for global chemical transport models: Model description and impact of nonsulfate aerosol particles.” *J. Geophys. Res.* 109: D18202. https://doi.org/10.1029/2003JD004405

Heyn, I., K. Block, J. Mülmenstädt, E. Gryspeerdt, P. Kühne, M. Salzmann, and J. Quaas. 2017. "Assessment of simulated aerosol effective radiative forcings in the terrestrial spectrum." *Geophys. Res. Lett.*, 44: 1001–1007. https://doi.org/10.1002/2016GL071975

Hoesly, R. M., S. J. Smith, L. Feng, Z. Klimont, G. JanssensMaenhout, T. Pitkanen, J. J. Seibert, L. Vu, R. J. Andres, R. M. Bolt, T. C. Bond, L. Dawidowski, N. Kholod, J.-I. Kurokawa, M. Li, L. Liu, Z. Lu, M. C. P. Moura, P. R. O'Rourke, and Q. Zhang. "Historical (1750–2014) anthropogenic emissions of reactive gases and aerosols from the Community Emissions Data System (CEDS)." *Geosci. Model Dev.*, 11, 369–408. https://doi.org/10.5194/gmd-11-369-2018.

Jeggle, K., D. Neubauer, H. Binder, and U. Lohmann. 2025. "Cirrus formation regimes – data-driven identification and quantification of mineral dust effect." *Atmos. Chem. Phys.*, 25, 7227–7243. https://doi.org/10.5194/acp-25-7227-2025

Kinne, Stefan. "Aerosol radiative effects with MACv2." *Atmospheric Chemistry and Physics* 19, no. 16 (2019): 10919-10959.

Liu, X., Penner, J.E. and Herzog, M., 2005. Global modeling of aerosol dynamics: Model description, evaluation, and interactions between sulfate and nonsulfate aerosols. *Journal of Geophysical Research: Atmospheres*, *110*(D18).

Liu, X., R. C. Easter, S. J. Ghan, R. Zaveri, P. Rasch, X. Shi, J. F. Lamarque, S. Gettelman, H. Morrison, F. Vitt, and A. Conley. 2012. "Toward a minimal representation of aerosols in climate models: Description and evaluation in the Community Atmosphere Model CAM5." *Geoscientific Model Development*, 5 (3): 709–739.

Liu, X., P-L. Ma, H. Wang, S. Tilmes, B. Singh, R. C. Easter, S. J. Ghan, and P. J. Rasch. "Description and evaluation of a new four-mode version of the Modal Aerosol Module (MAM4) within version 5.3 of the Community Atmosphere Model." *Geoscientific Model Development* 9, no. 2 (2016): 505-522.

Mahfouz, N., H. Beydoun, J. Mülmenstädt, N. Keen, A. C. Varble, L. Bertagna, P. Bogenschutz, A. Bradley, M. W. Christensen, T. C. Clevenger, A. Donahue, J. Fast, J. Foucar, J.-C. Golaz, O. Guba, W. Hannah, B. Hillman, R. Jacob, W. Lin, P.-L. Ma, Y. Qian, B. Singh, C. Terai, H. Wang, M. Wu, K. Zhang, A. Gettelman, M. Taylor, L. R. Leung, P. Caldwell, and S. Burrows. 2025. "Prescribing the aerosol effective radiative forcing in the Simple Cloud-Resolving E3SM Atmosphere Model v1." *Atmos. Chem. Phys.* 25, 15105–15120, https://doi.org/10.5194/acp-25-15105-2025

van Marle, M. J. E., S. Kloster, B. I. Magi, J. R. Marlon, A.-L. Daniau, R. D. Field, A. Arneth, M. Forrest, S. Hantson, N. M. Kehrwald, W. Knorr, G. Lasslop, F. Li, S. Mangeon, C. Yue, J. W. Kaiser, and G. R. van der Werf. 2017. "Historic global biomass burning emissions for CMIP6 (BB4CMIP) based on merging satellite observations with proxies and fire models (1750–2015)." *Geosci. Model Dev*., 10: 3329–3357. https://doi.org/10.5194/gmd-10-3329-2017

Rasch, P. J., S. Xie, P. L. Ma, W. Lin, H. Wang, Q. Tang, S. M. Burrows, P. Caldwell, K. Zhang, R. C. Easter, P. Cameron-Smith, B. Singh, H. Wan, J.-C. Golaz, B. E. Harrop, E. Roesler, J. Bacmeister, V. E. Larson, K. J. Evans, Y. Qian, M. Taylor, L. R. Leung, Y. Zhang, L. Brent, M. Branstetter, C. Hannay, S. Mahajan, A. Mametjanov, R. Neale, J. H. Richter, J.-H. Yoon, C. S. Zender, D. Bader, M. Flanner, J. G. Foucar, R. Jacob, N. Keen, S. A. Klein, X. Liu, A.G. Salinger, M. Shrivastava, and Y. Yang. 2019. "An overview of the atmospheric component of the

Energy Exascale Earth System Model." *Journal of Advances in Modeling Earth Systems* 11 (8): 2377–2411.

Textor, C., M. Schulz, S. Guibert, et al. 2006. "Analysis and quantification of the diversities of aerosol life cycles within AeroCom." *Atmos. Chem. Phys.* 6: 1777–1813. https://doi.org/10.5194/acp-6-1777-2006

Viovy, N. 2018. *CRUNCEP Version 7 - Atmospheric Forcing Data for the Community Land Model. NSF National Center for Atmospheric Research*. https://doi.org/10.5065/PZ8F-F017

Wang, H., R. C. Easter, R. Zhang, P. L. Ma, B. Singh, K. Zhang, D. Ganguly, P. J. Rasch, S. M. Burrows, S. J. Ghan, and S. Lou. 2020. "Aerosols in the E3SM Version 1: New developments and their impacts on radiative forcing." *Journal of Advances in Modeling Earth Systems* 12 (1): p.e2019MS001851.

Wang, M. H., J. E. Penner, and X. H. Liu. 2009. "Coupled IMPACT aerosol and NCAR CAM3 model: Evaluation of predicted aerosol number and size distribution." *J. Geophys. Res.-Atmos.* 114: D06302. https://doi.org/10.1029/2008JD010459

Xie, Shaocheng, Christopher R. Terai, Hailong Wang, Qi Tang, Jiwen Fan, Susannah Burrows, Wuyin Lin et al. "The energy exascale Earth system model version 3: 1. Overview of the atmospheric component." *Journal of Advances in Modeling Earth Systems* 17, no. 10 (2025): e2025MS005120.

Pacific Northwest National Laboratory

902 Battelle Boulevard
P.O. Box 999
Richland, WA 99354

1-888-375-PNNL (7665)

www.pnnl.gov